Multiple wavelength diffractive imaging

Bo Chen,[1] Ruben A. Dilanian,[1] Sven Teichmann,[2] Brian Abbey,[1] Andrew G. Peele,[3] Garth J. Williams,[1] Peter Hannaford,[2] Lap Van Dao,[2] Harry M. Quiney,[1] and Keith A. Nugent[1]

[1]*ARC Centre of Excellence for Coherent X-ray Science, School of Physics, The University of Melbourne, Victoria, 3010, Australia*

[2]*ARC Centre of Excellence for Coherent X-ray Science and Centre for Atom Optics and Ultrafast Spectroscopy, Swinburne University of Technology, Hawthorn, Victoria, 3122, Australia*

[3]*ARC Centre of Excellence for Coherent X-ray Science, Department of Physics, La Trobe University, Bundoora, Victoria, 3086, Australia*

(Received 19 September 2008; published 6 February 2009)

We demonstrate coherent diffraction imaging using multiple harmonics from a high-harmonic generation source. An algorithm is presented that builds the known incident spectrum into the reconstruction procedure with the result that the useable flux is increased by more than an order of magnitude. Excellent images are obtained with a resolution of (165 ± 5) nm and compare very well with images from a scanning electron microscope.

DOI: 10.1103/PhysRevA.79.023809 PACS number(s): 42.30.Rx, 42.25.Kb, 42.30.Va, 42.55.Vc

Soft x-ray microscopy is an important imaging technique that is currently reliant on the routine availability of access to synchrotron sources. However, the possibility of sources that enable small-scale x-ray microscopes [1] is helping drive the development of alternative x-ray sources such as x-ray lasers [2], compact synchrotron sources [3], and high-harmonic generation (HHG) sources [4].

The development of x-ray microscopy for the smaller scale laboratory has, to a great extent, concentrated on the development of bright but compact x-ray sources. It is implicitly assumed that imaging will require a high degree of spatial and temporal coherence, driven by the inherent chromaticity of diffractive optics [5] or, the need for spatial [6] and temporal [7] coherence in diffraction based methods. If the light is not completely coherent, a coherent component is selected [8–10], a process that is inherently wasteful of photons and which further drives the need for brighter sources. The underlying problem is that the phase-space acceptances of imaging systems using diffractive optics [1] or coherent diffraction [8,9] are not well matched to the phase space of the light delivered by tabletop sources. A better match between the phase space of the incident light and the image formation method will provide corresponding efficiencies in the utilization of the source.

In this paper we demonstrate coherent diffraction imaging that simultaneously uses multiple wavelengths, in a sense this is the spectral analogue of recent developments in x-ray holographic imaging that use multiple [11] or complex [12] reference waves. Our method is well matched to the low temporal coherence, high spatial coherence [4] optical field produced by an HHG source. Our method involves a modified iterative reconstruction algorithm that enables high quality diffractive imaging using all of the photons from an HHG source, and yields an order of magnitude improvement in the efficiency of the use of photons in an HHG-based tabletop x-ray microscope. We believe that this result will bring the prospect of a tabletop high-resolution x-ray microscope significantly closer.

A schematic of the experiment is shown in Fig. 1(a). The 5 mJ, 30 fs laser pulses centered at a wavelength of 805 nm are generated by a 1 kHz multistage multipass chirped-pulse amplifier system pumped by three solid state diode lasers. The laser pulses are focused by a lens with focal length 500 mm into a semi-infinite gas cell (300 mm length) with a glass window at the entrance and a 200 μm pinhole at the exit. The pressure of argon gas in the cell is kept at 25 torr with continuous flow. The small exit pinhole is used to isolate the vacuum chamber from the argon gas-filled cell. The pressure in the vacuum chamber is kept at $<1\times10^{-2}$ torr outside the gas cell and at $\sim10^{-4}$ torr in the experimental chamber where the sample is located. The optimal interaction length can be chosen through variation of the position of the focus point relative to the exit pinhole. The diameter of an aperture, which is placed in the path of the laser beam before the focusing lens, can be used to control the effective F-number, the spatial quality of the laser beam, and the peak intensity in the focus area. The experimental system is arranged so that the HHG emission at the sample is confined to just a few orders [13].

The sample is mounted on a holder inside an experimental vacuum chamber. The diffraction pattern is detected with a CCD camera (Princeton Instruments) containing a 1340×1300 array of 20 μm pixels. The distance between the CCD and the sample is 6.5 cm. To further reduce the scattered light an aperture with diameter of 5 mm is placed directly downstream from the sample.

A monochromator was not used in this experiment and so the illumination contained several harmonics. The spectrum of the incident beam was determined via a maximum entropy method analysis of the fringes produced by a Young's two-slit experiment [14]. A sample spectrum is shown in Fig. 1(b). This method also yields a reliable estimate of the spatial coherence length, which was found to be significantly greater than 20 μm.

As a test target we have used a carbon grid windowed by a pinhole. A carbon film of nominally 40 nm thickness with an array of 2 μm diameter circular holes with a center-to-center spacing of 3 μm was placed in front of an opaque steel pinhole with a diameter of 20 μm. The carbon film is not completely opaque to the incident light and so the diffracted spectrum will be altered after transmission through the foil. We here reconstruct the density distribution of the sample and use the known optical properties of carbon [15].

This data was acquired in two stages: The first consisted

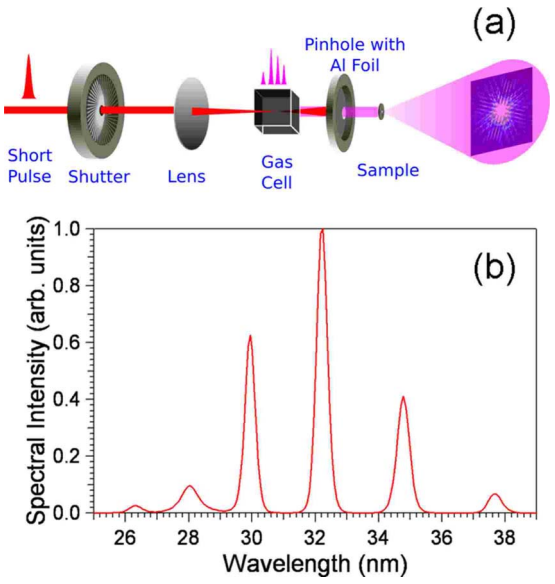

FIG. 1. (Color online) (a) Schematic of the HHG laser and diffraction imaging experimental setup. (b) HHG source spectrum deduced from the Young's double-slit experiment. The light incident on the sample consists of approximately six well-defined harmonics of the driving optical laser.

of 1000 frames of data each with an exposure time of 1.2 seconds. The short exposure time did not allow the acquisition of high-angle diffracted data. The second stage involved the acquisition of 30 data frames each with an exposure time of 78 seconds. The low scattering angle data in these frames was highly overexposed and the CCD was saturated in these regions. The two data sets were then normalized to each other and combined so as to retain the high-angle scatter from the long exposure data with the nonsaturated data from the short exposure time data; the total exposure time was 59 minutes. The resulting combined experimental diffraction pattern is shown in Fig. 2.

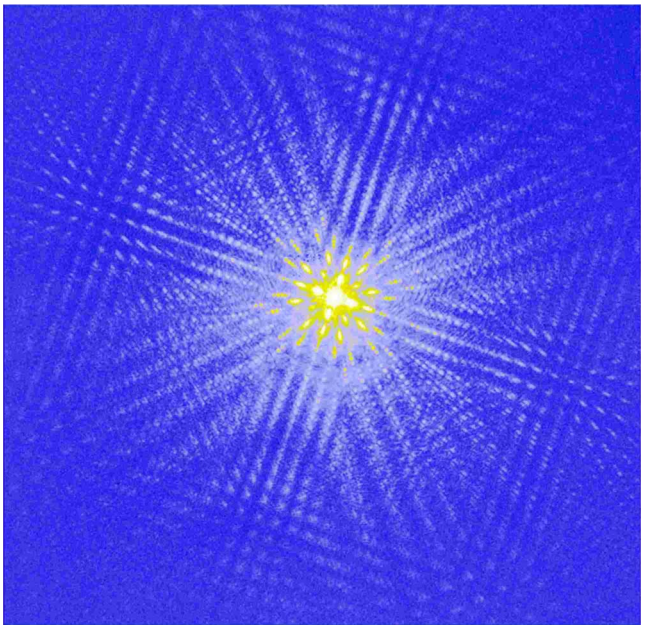

FIG. 2. (Color online) Diffraction data acquired from the sample. This consists of the combination of two different exposure times so as to allow for the measurement of the very intense low-angle scatter and the relatively low intensity high-angle scatter. The data is displayed on a highly nonlinear scale.

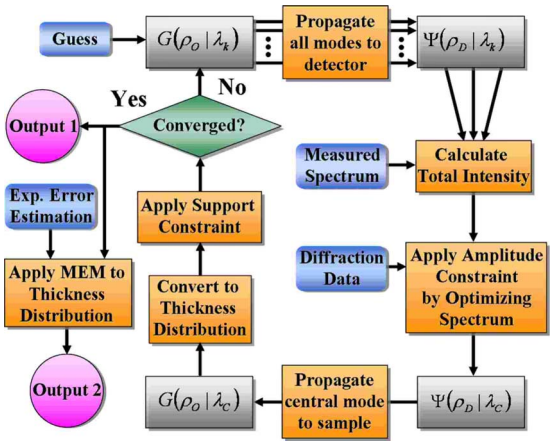

FIG. 3. (Color online) Flow diagram for the image reconstruction algorithm. The reconstruction takes place in two sections. The first, denoted output 1, is the image from the modified Gerchberg-Saxton iteration. The second, output 2, is a maximum entropy method refinement step.

The limiting factor in the exposure time is the ability to acquire the high-diffraction angle data, which took 39 minutes. The largest harmonic component contains approximately one-quarter of the energy in the complete incident spectrum, and an efficient monochromator system, such as wavelength-selective multilayer mirror, will have an efficiency of around 25% [8]. Hence we estimated that the use of multiple harmonics reduces the exposure time by a factor of ~16. The differences in the experimental arrangement between the present work and other reports [8] make detailed quantitative comparison of relative exposure times difficult.

Although the sample contains only a small number of periods within its finite extent, its diffraction pattern has a strong qualitative resemblance to the pattern that would be produced by an extended periodic sample. Close inspection reveals, however, that the pattern contains some important differences, key among them being that there is significant intensity in between, and structure to, the diffraction "spots." A second key feature is that the individual diffraction peaks themselves contain a series of peaks produced by each of the harmonics from the HHG source, so that the diffraction pattern is an incoherent superposition of the diffraction by each harmonic incident on the sample. We note that this diffraction pattern obeys the oversampling criterion [16] and that the finite size of the object is critical to our ability to obtain a reliable image reconstruction.

The reconstruction algorithm is schematically represented in the flow diagram shown in Fig. 3. We assume that the incident light has a spectrum distribution, $F(\lambda)$, consisting of a finite number of harmonics. We sample this spectrum into a set of N values (512 samples equally spaced in optical frequency), S_k; $k=1,2,\ldots,N$, and assume that there is negligible interference between each component. This is a good approximation for our exposure times, which are long com-

pared to the beat time between adjacent modes. The observed intensity distribution is therefore the incoherent superposition of the diffraction patterns from each spectral sample. We define ρ_D and ρ_O as position vectors in the detector and object planes, respectively.

The initial estimate for the object distribution was obtained from the autocorrelation function of the sample obtained by Fourier transforming the measured diffraction intensity. The background was subtracted off the autocorrelation data. As the data is very close to that of a periodic structure, the remaining part of the autocorrelation function has a periodic component. The central 3×3 periods of the data were isolated and used to tile all of the image space, initially without regard to the known support information.

The exit wave field $G(\rho_O|\lambda_k)$ leaving an object consisting of a single known material with complex wavelength-dependent refractive index $n(\lambda)$ and illuminated with a coherent plane wave with wavelength λ_k can be written in terms of the thickness function, $T(\rho_0)$, $G(\rho_O|\lambda_k)=\exp[i\frac{2\pi}{\lambda_k}n(\lambda_k)T(\rho_O)]$. For a single wavelength, λ_k, the propagation of $G(\rho_O|\lambda_k)$ to the detector plane can be described using the paraxial free-space far-field approximation $\Psi(\rho_D|\lambda_k)\sim-\frac{i}{\lambda_k Z}\hat{F}_{\lambda_k}\{G(\rho_O|\lambda_k)\}$, where $\Psi(\rho_D|\lambda_k)$ is the wave field with this wavelength at the detector plane, $\hat{F}_{\lambda_k}$ denotes the Fourier transform operator scaled according to the wavelength and Z is the object-detector distance. Assuming no interference between wavelength components, the estimated intensity at the detector plane is given by $I_T(\rho_D)=\Sigma_{k=1}^{N}S_k|\Psi(\rho_D|\lambda_k)|^2$, where S_k are the spectral weightings previously defined.

The values of S_k are modified by the properties of the sample. Using the measured spectrum as a starting point, we fit the predicted intensity distribution to the measured intensity distribution via the distribution of spectral weights. We first create a cost function

$$\Omega=\frac{1}{2P}\sum_{j=1}^{P}[\sqrt{I_T(\rho_D)}-\sqrt{I_E(\rho_D)}]^2, \tag{1}$$

where $I_E(\rho_j)$ is the experimental intensity distribution, and P is the total number of experimental points. The spectrum optimization procedure is based on the gradient descent optimization and is reached through several hundred iterations.

The amplitude constraint is defined through

$$\Psi(\rho_D|\lambda_k)=\Psi(\rho_D|\lambda_k)\frac{\sqrt{\tilde{I}(\rho_D|\lambda_k)}}{|\Psi(\rho_D|\lambda_k)|}. \tag{2}$$

Each of the modes must individually satisfy the support constraint and so only one mode is propagated back to the sample, to be used as the basis for the update of the estimate $T(\rho_o)$ in the next iterative cycle.

A scanning electron microscope image of the sample is shown in Fig. 4(a). The resulting reconstruction is shown in Fig. 4(b) which used the support indicated by the dotted circle shown. It can be seen to be an excellent reconstruction. The reconstruction in Fig. 4(b) was further used as the starting point for a maximum entropy method (MEM) reconstruction algorithm [17] so as to eliminate all the features not demanded by the data; the refined reconstruction is shown in Fig. 4(c), showing excellent agreement with the image in Fig. 4(a).

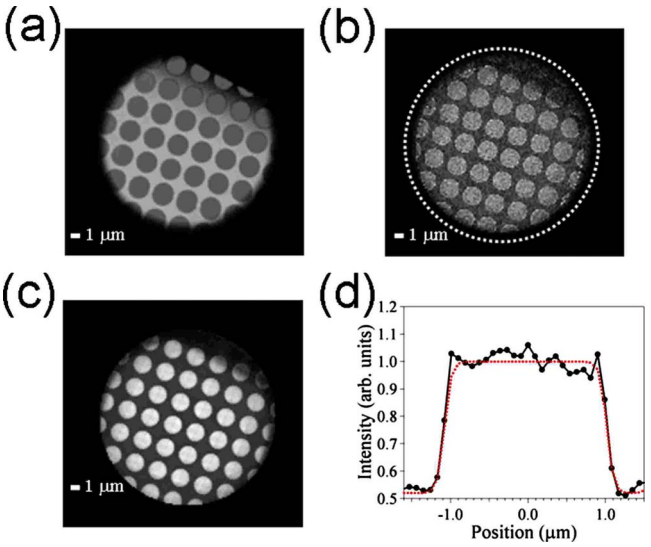

FIG. 4. (Color online) (a) A scanning electron microscope image of the sample used in the diffraction experiment. (b) Output from the first stage, Gerchberg-Saxton, of the iterative scheme. The dotted circle indicates the support assumed in the reconstruction. (c) Output after the maximum entropy methods step of the data reconstruction. (d) The line out through one of the small pinholes shows the curve fitting used to estimate the spatial resolution of (165 ± 5) mm. This resolution is consistent with diffraction-limited imaging at a wavelength of about 35 nm with this experimental geometry.

The MEM refinement produces a much smoother image but some of the detail in the sample is lost, indicating that the algorithm is probably underfitting the data due to an overestimate of the noise level. The faint crosslike structure that can be discerned within each of the individual pinholes probably has a related origin. Note that the otherwise circular pinhole is cut off by a piece of polymer across the top on the images in Fig. 4. This polymer is opaque to the electrons, but it is possible to see the individual pinholes through this structure in the x-ray image, consistent with the greater penetration of this radiation. Also note that the pinhole array extends slightly further for the x-ray image than for the electron image, and that the edge of the larger pinhole is sharper in the x-ray image. We attribute these features to the x rays having greater penetration than the electrons and the x-ray image having a greater depth of field than the electron image.

The reconstruction algorithm directly returned a value for the average sample thickness of the carbon foil of (37 ± 2) nm, consistent with its nominal thickness. We fitted a sigmoid to the edge distributions in the image [Fig. 4(d)] to obtain an estimated full width at half-maximum for the resolution function of (165 ± 5) nm. If the resolution, Δ, is determined by the relationship $\Delta=0.94\lambda/NA$ (Sparrow criterion), where NA is the numerical aperture of the detector, then the observed resolution is consistent with an effective wavelength of (35 ± 1) nm, close to the central peak wavelength in the incident spectrum.

In conclusion, a study demonstrating diffractive imaging using multiple-wavelength sources has been presented. The reconstruction from such data is not possible using iterative methods that implicitly assume perfect coherence. These results will enable better utilization of HHG sources for diffractive imaging. Our approach will also facilitate the reconstruction of images in the presence of the moderate longitudinal coherence expected in the output from unseeded x-ray free electron lasers, in which case the longitudinal coherence properties of these sources should not pose any obstacle to the diffractive imaging of very large samples or, perhaps, molecular clusters.

The authors acknowledge support from the Australian Research Council and the Victorian government Strategic Technology Innovation initiative.

[1] M. Berglund *et al.*, J. Microsc. **197**, 268 (2000).
[2] B. R. Benware, C. D. Macchietto, C. H. Moreno, and J. J. Rocca, Phys. Rev. Lett. **81**, 5804 (1998).
[3] P. Sprangle *et al.*, J. Appl. Phys. **72**, 5032 (1992).
[4] R. A. Bartels *et al.*, Science **297**, 376 (2002).
[5] J. Kirz, C. Jacobsen, and M. Howells, Q. Rev. Biophys. **28**, 33 (1995).
[6] G. J. Williams, H. M. Quiney, A. G. Peele, and K. A. Nugent, Phys. Rev. B **75**, 104102 (2007); J. C. H. Spence, U. Weierstall, and M. Howells, Ultramicroscopy **101**, 149 (2004).
[7] S. P. Hau-Riege, Opt. Express **16**, 2840 (2008).
[8] R. L. Sandberg *et al.*, Phys. Rev. Lett. **99**, 098103 (2007).
[9] R. L. Sandberg *et al.*, Proc. Natl. Acad. Sci. U.S.A. **105**, 24 (2008).
[10] D. Shapiro *et al.*, Proc. Natl. Acad. Sci. U.S.A. **102**, 15343 (2005); P. Thibault *et al.*, Acta Crystallogr., Sect. A: Found. Crystallogr. **62**, 248 (2006).
[11] W. F. Schlotter *et al.*, Appl. Phys. Lett. **89**, 163112 (2006).
[12] S. Marchesini *et al.*, Nat. Photonics **2**, 560 (2008).
[13] L. Van Dao, S. Teichmann, and P. Hannaford, Phys. Lett. A **372**, 5254 (2008).
[14] R. A. Dilanian *et al.*, Opt. Lett. (to be published).
[15] Lawrence Berkeley National Laboratory Center for X-ray Optics, X-ray optics tools, http://www-cxro.lbl.gov/index.php?content=/tools.html
[16] J. Miao, D. Sayre, and H. N. Chapman, J. Opt. Soc. Am. A Opt. Image Sci. Vis **15**, 1662 (1998).
[17] S. F. Gull and G. J. Daniell, Nature (London) **272**, 686 (1978).